Steady Viscous Flow in a Trapezoidal Cavity

William D. McQuain, Calvin J. Ribbens,
C.-Y. Wang, and Layne T. Watson

TR 92-58

Department of Computer Science
Virginia Polytechnic Institute and State University
Blacksburg, Virginia 24061

December 22, 1992

Steady Viscous Flow in a Trapezoidal Cavity

WILLIAM D. MCQUAIN, CALVIN J. RIBBENS
Department of Computer Science, Virginia Polytechnic Institute & State University, Blacksburg, VA 24061, U.S.A.

C.-Y. WANG
Departments of Mathematics and Mechanical Engineering, Michigan State University, East Lansing, MI 48824, U.S.A.

AND

LAYNE T. WATSON
Departments of Computer Science and Mathematics, Virginia Polytechnic Institute & State University, Blacksburg, VA 24061-0106, U.S.A.

The flow in a trapezoidal cavity (including the rectangular and triangular cavities) with one moving wall is studied numerically by finite differences with special treatment in the corners. It is found that streamlines and vorticity distributions are sensitive to geometric changes. The mean square law for core vorticity is valid for the rectangle but ceases to be valid for the triangular cavity.

1. INTRODUCTION

The study of the flow in an enclosure driven by the tangential motion of a segment of the boundary is extremely important. Physically the flow represents recirculating viscous motion in the wake of bluff bodies, behind abrupt constrictions in channel flow or flow inside open cavities on a wall due to outside disturbances. Owing to the nonlinearity of the Navier-Stokes equations, the problem cannot be solved analytically, and only a "mean square law" governing the interior circulation for infinite Reynolds numbers has been proposed [1]. Since the enclosure geometry is simple and finite, the problem has also been an important test case for numerical computational schemes.

The most numerically studied case is the square cavity with three solid boundaries and the fourth boundary moving at a constant speed. A variety of methods have been used—finite differences, false transients, multi-grid methods, etc. (e.g., Burggraf [2], Ghia et al. [3], Shreiber and Keller [4], and reviews by Tuann and Olson [5], Gustafson and Halasi [6]). Although there are still some minor discrepancies in the results, the square cavity problem is considered essentially solved. In general there is a dominant recirculating eddy generated by the moving wall and two smaller counter-rotating eddies at the stagnant corners. For high Reynolds numbers the vorticity in confined to a boundary layer and the interior vorticity is approximately constant.

However, the result for a square cavity may not be applied to other important geometries such as a trapezoidal cavity (including the triangular cavity). In fact the latter shapes are more common in practice. For example, it is much easier to mill a trapezoidal groove, which is wider at the opening, than a square one. Also, triangular grooves are necessary for flexible corrugated tubes [7] and for heat transfer enhancement [8].

The aims of this paper are as follows. First, we would like to determine the effects of geometry on the physics of cavity flow. In particular, we examine the continuous change of streamlines and vorticity from the rectangle, through trapezoids, to the triangle. Second, nonrectangular geometry, especially the triangle, requires special numerical treatment. We introduce a successful method and discuss our experiences with the problems associated with other traditional methods.

2. FORMULATION

Let Ω be the isosceles trapezoid with corners $(\delta a, 0)$, $((2\sqrt{3}-\delta)a, 0)$, $(2\sqrt{3}a, 3a)$, $(0, 3a)$, where $0 \le \delta \le \sqrt{3}$, and let $\partial\Omega$ be the boundary of Ω. The two-dimensional steady Navier-Stokes equations are

$$u'u'_{x'} + v'u'_{y'} = -\frac{1}{\rho}p'_{x'} + \nu\left(u'_{x'x'} + u'_{y'y'}\right), \tag{1}$$

$$u'v'_{x'} + v'v'_{y'} = -\frac{1}{\rho}p'_{y'} + \nu\left(v'_{x'x'} + v'_{y'y'}\right), \tag{2}$$

$$u'_{x'} + v'_{y'} = 0. \tag{3}$$

Here u', v' are velocity components in the Cartesian x', y' directions, ρ is the density, p' is the pressure, and ν is the kinematic viscosity. The boundary conditions are that velocity is constant U along the top (wider base) of the trapezoid, the velocity is zero on fixed sides, and velocities are bounded inside Ω. We normalize all velocities by U, the pressure by ρU^2, the lengths by a, and drop primes. Define a stream function ψ by

$$u = \psi_y, \qquad v = -\psi_x. \tag{4}$$

The governing equations in Ω become

$$\nabla^4\psi = R\left(\psi_y\nabla^2\psi_x - \psi_x\nabla^2\psi_y\right), \tag{5}$$

where ∇^2 is the Laplacian operator and R is the Reynolds number Ua/ν. The boundary conditions become

$$\psi = 0 \text{ on all four sides of } \Omega, \tag{6}$$

and

$$(\psi_y, -\psi_x)\cdot\mathbf{T} = \begin{cases} 1, & \text{for the top side,} \\ 0, & \text{for the other three sides,} \end{cases} \tag{7}$$

where $\mathbf{T}$ is a unit vector tangent to the boundary pointing in the direction of motion (clockwise). Equation (7) determines the magnitude of the velocity vector $(\psi_y, -\psi_x)$. The direction of the velocity is already determined (up to sign) by (6), since $\psi = 0$ on $\partial\Omega$ implies $\nabla\psi = (\psi_x, \psi_y)$ is normal to a side; and thus the velocity, which is normal to $\nabla\psi$, must be tangent to the boundary. For the isosceles trapezoid Ω considered here, equation (6) can be written

$$\begin{aligned} \psi_y &= 1, \text{ on the top side,} \\ \psi_y &= 0, \text{ on the bottom side,} \\ 3\psi_x - \delta\psi_y &= 0, \text{ on the right side,} \\ 3\psi_x + \delta\psi_y &= 0, \text{ on the left side.} \end{aligned} \tag{8}$$

3. NUMERICAL METHODS

We apply a Newton-like iteration to equation (5). It is well known that if Newton's method converges to the root of a nonlinear equation, it does so rapidly. However, a good initial guess

is usually needed for convergence to occur. We use a very simple initial guess, namely a quartic polynomial constructed to be zero on $\partial\Omega$. For the isosceles trapezoid we choose

$$\psi^{(0)}(x,y) = y(3-y)(3x-\delta y-6\sqrt{3}+3\delta)(3x+\delta y-3\delta), \tag{9}$$

while for the unit square discussed in Section 3.2 below we use

$$\psi^{(0)}(x,y) = xy(1-x)(y-1). \tag{10}$$

Rapid convergence is achieved for $R = 1$ in all cases with sufficiently fine grids. Solutions for higher Reynolds number in a given case are computed by using as initial guess a solution for a slightly smaller R for the same case.

A Newton-like linearization of the nonlinear operator in Equation (5) results in the following linear fourth order PDE to be solved at each iteration:

$$\nabla^4\psi - R\left(\psi_y^{(i)}\nabla^2\psi_x + \nabla^2\psi_x^{(i)}\psi_y - \psi_x^{(i)}\nabla^2\psi_y - \nabla^2\psi_y^{(i)}\psi_x\right) = -R\left(\psi_y^{(i)}\nabla^2\psi_x^{(i)} - \psi_x^{(i)}\nabla^2\psi_y^{(i)}\right), \tag{11}$$

where $\psi^{(i)}$ is the approximate solution from the previous step. See Ribbens et al. [9] for a more detailed derivation of (11). At each step of the outer iteration we must solve the linear problem defined by Equations (6), (8), and (11). Notice that linearization precedes discretization. One could also discretize first and then deal with the resulting system of nonlinear equations, but the two approaches are essentially equivalent.

3.1 Finite difference methods for the limiting cases

The limiting case of our trapezoid as $\delta \to 0$ is a $2\sqrt{3} \times 3$ rectangle, which is nearly, but not identical with, the square case. The parametric mapping that goes exactly from an equilateral triangle through isosceles trapezoids to a square is more complicated than our mapping, which preserves the moving side to depth aspect ratio $(2/\sqrt{3})$. An efficient numerical technique for solving the related driven square cavity problem is described by Schreiber and Keller [4]. The classical driven cavity problem describes steady viscous incompressible flow in the unit square, with one side moving. The technique employed in [4] is based on central differences and a uniform rectangular grid, yielding a discretization with second order accuracy. The difference formulas used to approximate the derivative terms in both the PDE and the boundary conditions are centered. A 13 point stencil is required for the fourth-order derivatives. In order to impose the PDE at grid points just inside the region, "fictional" grid points just exterior to the boundary are required, but the unknown ψ values at these exterior grid points are determined by imposing the normal derivative boundary condition at nearby boundary grid points. The technique in [4] also includes continuation in the Reynolds number, a special sparse direct factorization scheme for the resulting linear systems, and Richardson extrapolation for improved accuracy. The numerical method for our limiting rectangle case is essentially the same as that of [4] for the square, and need not be described further.

The other limiting case as $\delta \to \sqrt{3}$ of a triangle is entirely different. The triangle, unlike a trapezoid, cannot be mapped onto a square without a singularity. We considered modifying the approach of Schreiber and Keller for the triangle problem. Unfortunately, the equilateral triangle presents considerable difficulties under such an approach. As in [4], we can introduce grid points just external to the region and then eliminate them by hand by imposing the derivative boundary

condition (8) at boundary grid points. The corners require special treatment, and also force the use of nonsymmetric 18 point stencils for the PDE at the interior points nearest all three corners. For the remaining interior grid points the standard 13 point finite difference stencil suffices. Pictures of these stencils and complete details for the triangle case are in [11].

Despite our relatively straightforward generalization of the technique of Schreiber and Keller, the linear systems generated by the method just described are so ill conditioned that accurate numerical solutions are virtually impossible. In fact, for moderately fine grids (e.g., 49 vertical grid lines and 25 horizontal grid lines) the systems are numerically singular, with condition numbers in excess of 10^{13}. The problem is related to the special treatment required in the corners and to the overlapping stencils needed for the derivative boundary equations along the left and right sides. On a test problem, if we assume the external solution values are known, so that neither the one-sided stencils nor the derivative boundary equations are needed, the linear systems become quite well conditioned (e.g., 10^3 for the case mentioned above). We did not pursue further the causes of the ill conditioning or seek remedies, as the approach described in [11] proved successful. However, it is interesting to note the significant problems that arise in modifying the straightforward difference method of Schreiber and Keller for the triangle.

In a previous paper [9] we described a numerical technique for solving the related problem of flow induced in an elliptic region by the boundary moving at constant velocity. In that work our numerical approach was based on collocation with Hermite cubic basis functions, and we defined the problem as a coupled system of two second order equations in two unknowns (stream function and vorticity). This strategy proved quite successful and yielded accurate solutions for Reynolds number up to 1000 and for ellipses with aspect ratio up to 5.

An analogous strategy for the present problem is not successful, however. As in the finite difference method described above, special problems near the corners lead to nearly singular linear systems, and in fact to exactly singular systems if the collocation points are not chosen carefully. Our experience is that this extreme ill conditioning causes inaccuracies in the approximate solution, and prevents the Newton iteration from converging for all but the smallest Reynolds numbers. Neither collocation nor centered finite differences applied to the system of two second order equations was successful.

The ultimate resolution of the numerical difficulties for the triangle case is to map the equilateral triangle to an isosceles right triangle, and develop new nonsymmetric finite difference stencils for the right triangle. In particular, we introduced a change of variables

$$\xi = x + (y+2)/\sqrt{3} \qquad \text{and} \qquad \eta = 2(1-y)/\sqrt{3},$$

so that our computational region is a right triangle with corners $(0,0)$, $(2\sqrt{3},0)$, and $(0,2\sqrt{3})$. Fortunately, this transformation preserves the Neumann nature of the boundary conditions (8) (not true if the triangle is scalene!), and the resulting linear systems are well conditioned. Further details of this transformation and the necessary skewed finite difference stencils are in [11].

3.2. Finite differences for the trapezoid

The generic trapezoid case is considerably simpler than the limiting triangle case. The trapezoid can be mapped smoothly onto the unit square by

$$\xi = \frac{\delta y + 3x - 3\delta}{2(\delta y + 3\sqrt{3} - 3\delta)} \qquad \text{and} \qquad \eta = \frac{y}{3},$$

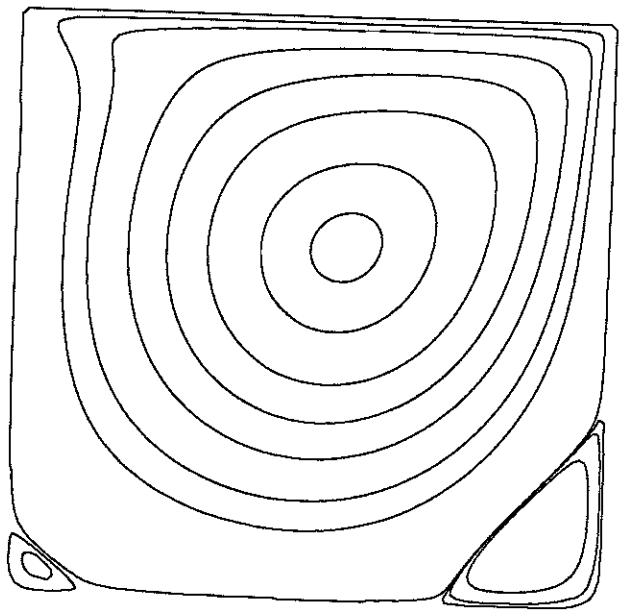

FIG. 1. Cavity flow in a square, R=115.47.

so that the computational region is the unit square $\tilde{\Omega}$ with lower left corner $(0,0)$. The transformed PDE operator in ξ, η is a very general one indeed, since the chain rule produces terms of up to total (derivative) degree 4 with coefficients depending on the coefficients of the original problem and on the transformation. Deriving the transformed coefficients and new difference formulas for all of these derivative terms by hand would be extremely tedious. We found the process reasonably straightforward, however, using the symbolic computational facilities of Mathematica [12].

The transformed derivative boundary conditions are still simply normal derivative conditions on $\tilde{\psi}$, the unknown in $\tilde{\Omega}$ (i.e., a Neumann condition). As long as δ is not too close to $\sqrt{3}$, the resulting linear systems are well conditioned and the solution of the transformed PDE on $\tilde{\Omega}$ can proceed as in [4]. There are several possibilities for second order accurate finite difference stencils in the interior of the region. We chose to use the stencils developed in [11] rather than those from [4]; both are second order accurate.

To test the accuracy of our algorithm, we computed the streamlines for a $2\sqrt{3}$ square for $R = 115.47$, which is equivalent to $R = 400$ in the usual definition of Reynolds number, using the entire length of one side. Fig. 1 shows that our results, using a mesh size of 101, are identical to those of Schreiber and Keller [4].

4. THE STREAMLINES

Using our algorithm, the streamlines are computed for a variety of Reynolds numbers and cavity shapes. In Figs. 2–5 the streamline contour spacing is 0.02. Fig. 2 shows the streamlines for a $2\sqrt{3} \times 3$ rectangle ($\delta = 0$ case). The motion of the top boundary is from left to right, thus the primary eddy is clockwise. For $R = 1$ lateral symmetry exists, implying that nonlinear effects are unimportant. As R increases to 500 (equivalent to a conventional Reynolds number of 1732), the primary eddy becomes skewed. Similarly to the case of the square, the center of the eddy initially moves to the right, then down and towards the center. For larger R the secondary eddies at the stagnant corners become larger, and tertiary eddies begin to appear.

TABLE I

Properties of the center of the primary eddy, located at (x_c, y_c) with stream function value ψ_c and vorticity ζ_c.

R	x_c	y_c	ψ_c	ζ_c
Triangle ($\delta = \sqrt{3}$)				
1	1.749	2.460	.233	1.363
50	2.078	2.445	.237	1.464
100	2.061	2.355	.247	1.373
200	1.940	2.280	.260	1.272
350	1.905	2.265	.268	1.232
500	1.905	2.265	.269	1.250
Trapezoid ($\delta = (2/3)\sqrt{3}$)				
1	1.747	2.382	.267	1.200
50	2.110	2.319	.276	1.247
100	2.023	2.193	.290	1.105
200	1.907	2.105	.305	1.019
400	1.848	2.067	.315	.970
500	1.848	2.055	.317	.964
Trapezoid ($\delta = (1/3)\sqrt{3}$)				
1	1.747	2.294	.304	1.062
50	2.125	2.155	.321	1.018
100	1.965	1.954	.339	.873
200	1.878	1.853	.353	.789
400	1.834	1.777	.361	.741
500	1.819	1.765	.363	.730
Rectangle ($\delta = 0$)				
1	1.747	2.206	.340	.950
50	2.140	1.979	.365	.856
100	1.994	1.777	.383	.742
200	1.907	1.702	.396	.687
400	1.878	1.651	.403	.658
500	1.863	1.639	.405	.650

Fig. 3 shows the $\delta = 1/\sqrt{3}$ trapezoid. There are several effects of shortening the lower boundary. The center of the primary eddy is now closer to the moving boundary. At higher R the two secondary eddies at the stagnant corners tend to coalesce. Most important is the appearance of the third secondary eddy near the upper left corner. Fig. 4 shows a trapezoid with the lower base further shortened. The two lower secondary eddies easily coalesce into one.

Fig. 5 shows the streamlines for the triangle. Note that secondary and tertiary eddies exist at the lower corner even at low R. For higher R even quaternary eddies appear. These eddies alternate in sense and rapidly decrease in strength, not unlike those found in deep rectangular cavities [13].

5. THE VORTICITY DISTRIBUTION

The vorticity contour spacing in Figs. 6–9 is 0.5. Fig. 6 shows the vorticity distribution for the rectangle. For low R vorticity diffuses from the corners of the top boundary, where velocity

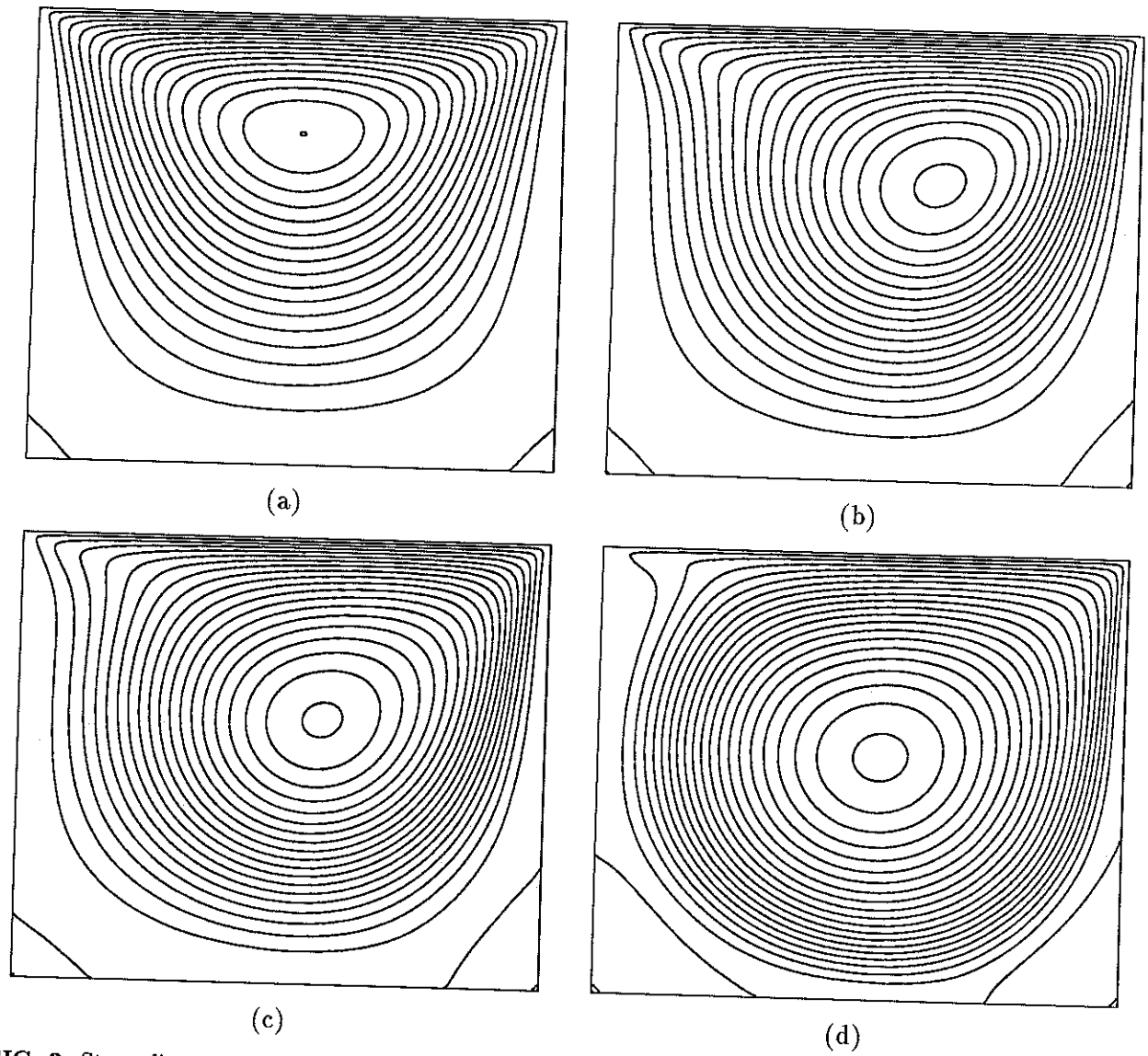

FIG. 2. Streamline patterns for the rectangle, δ=0, for R=1 (a), R=50 (b), R=100 (c), and R=500 (d).

discontinuities exist. As R is increased the vorticity is transported downstream, and concentrated near the top and right boundaries. At $R = 500$ vorticity in the core of the primary eddy becomes approximately constant. The vorticity distributions for trapezoids and the triangle are shown in Figs. 7–9. Notice that the constant vorticity core becomes smaller as δ increases.

Table 1 shows the location of the center of the primary eddy and the corresponding vorticity ζ_c. Note that ζ_c generally decreases with decreased δ and with increased R. At $R = 500$, ζ_c would represent the vorticity of the large core region.

In order to verify the mean square law, we derived the theoretical values for ζ_c at large Reynolds numbers (see Appendix II). Results are obtained only for the rectangle and equilateral triangle, since the general trapezoidal shape does not yield analytic solutions. For the rectangle we find the theoretical value $\zeta_c = 0.6071$, which differs by about 6.5% from our computed value of 0.650. For the triangle we obtain a theoretical value $\zeta_c = 1.054$, while the computed value is 1.250. The difference of 15.7% is unacceptable.

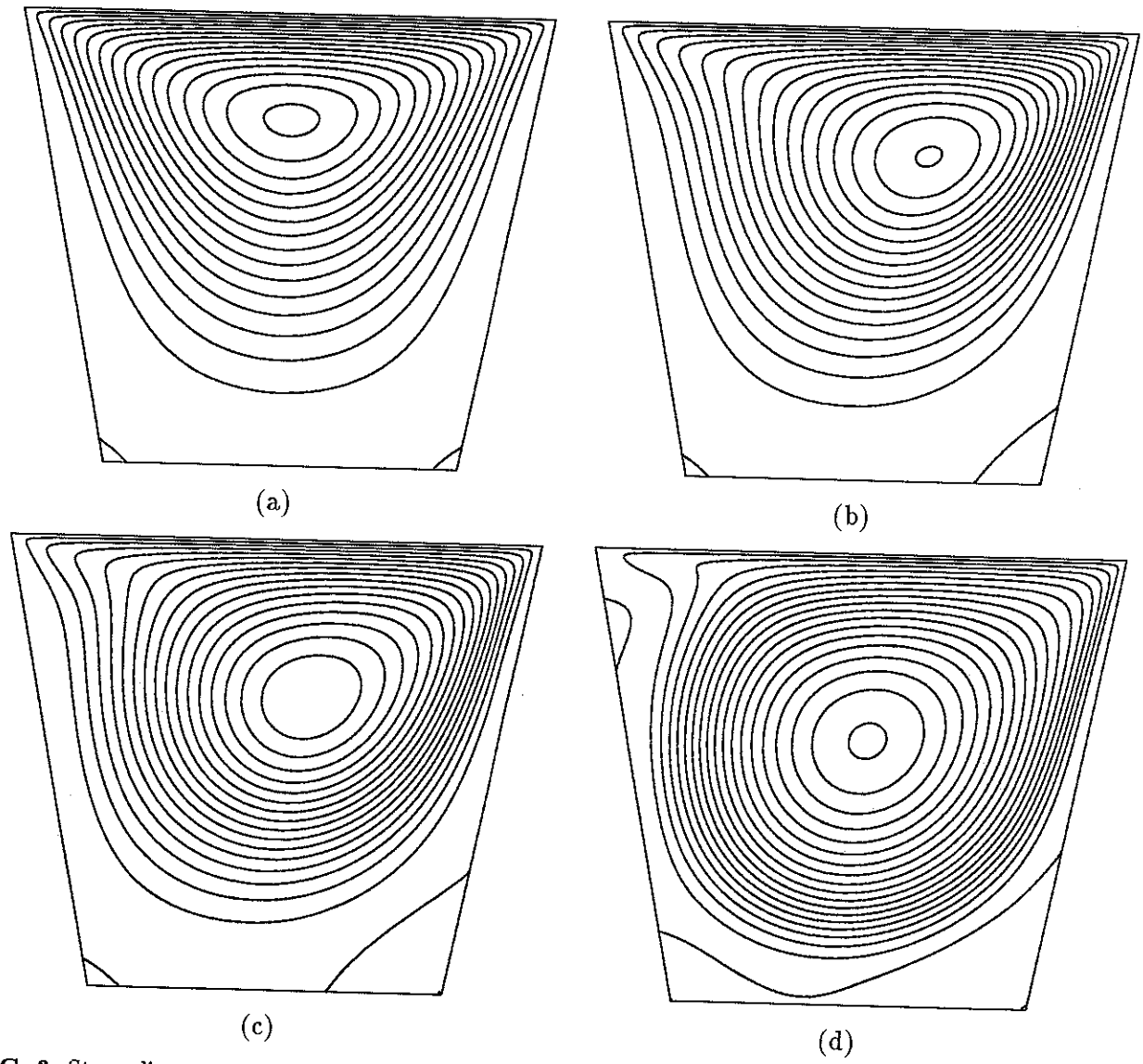

FIG. 3. Streamline patterns for the trapezoid, $\delta=1/\sqrt{3}$, for R=1 (a), R=50 (b), R=100 (c), and R=500 (d).

6. DISCUSSION AND CONCLUSIONS

We find the streamlines are altered as the geometry changes from a rectangle, through a series of trapezoids, to a triangle. The primary eddy becomes smaller, only partially filling the cavity. Due to its sharper and larger stagnant region, the triangle exhibits secondary, tertiary and quaternary eddies. Thus a triangular cavity would be comparatively less effective in the transport of mass and energy by convection.

The triangle is qualitatively different from the rectangle and trapezoid because, unlike the latter two, it cannot be mapped onto a square without a singularity. This necessitates a different numerical algorithm for the triangle case, and new finite difference stencils as in Appendix I. The same numerical approach and finite difference stencils as used for the trapezoid fail completely for the triangle.

The mean square law for vorticity at high Reynolds numbers seems to be valid for the square [14], the ellipse [9], and the rectangle studied in this paper, but fails for the triangle. The reason lies in the vorticity distribution. For the rectangle the vorticity is concentrated along the boundary

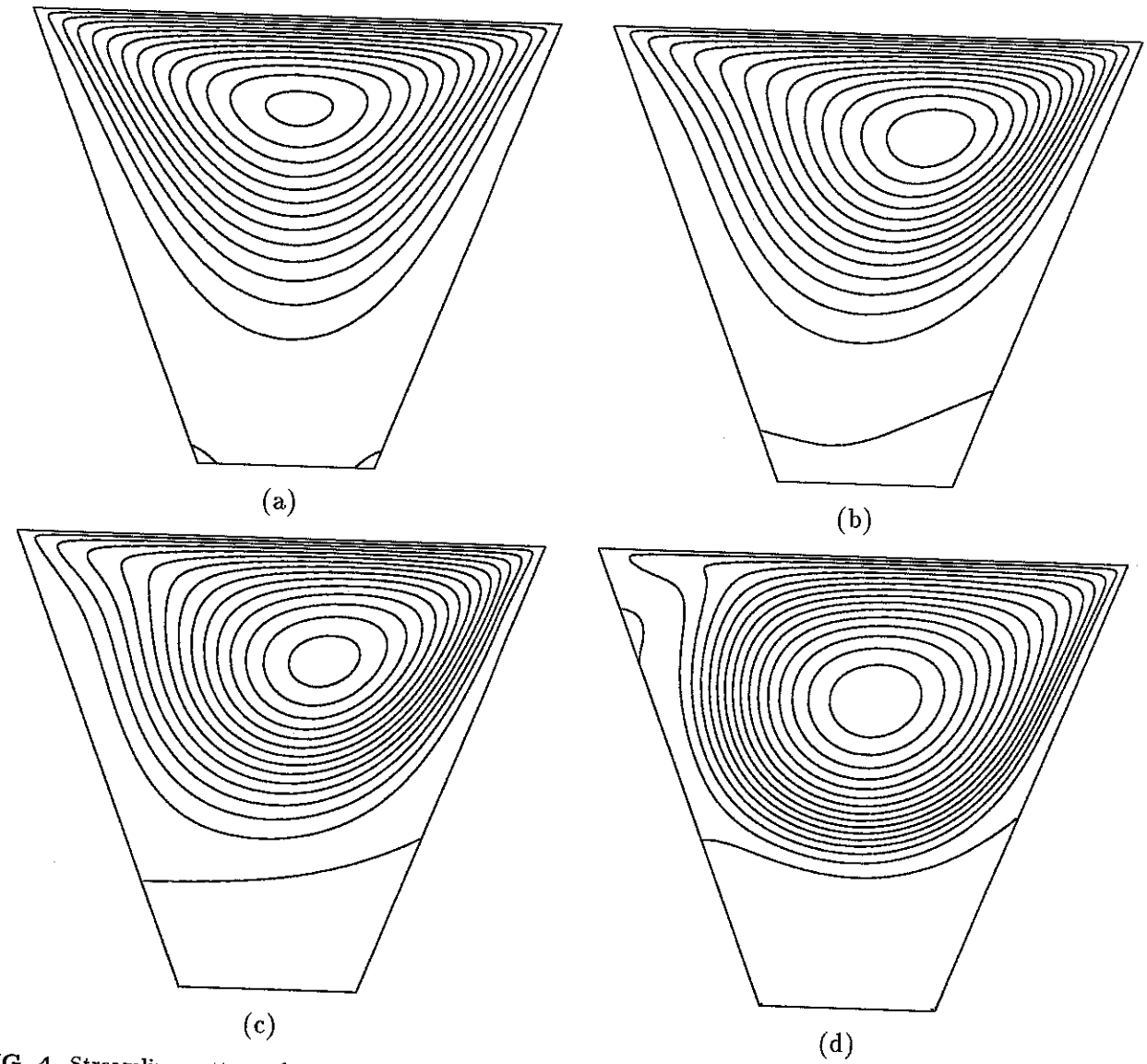

FIG. 4. Streamline patterns for the trapezoid, $\delta=2/\sqrt{3}$, for R=1 (a), R=50 (b), R=100 (c), and R=500 (d).

(Fig. 6d), thus fulfilling Batchelor's thin boundary layer assumption. For the triangle (and some trapezoids) the vorticity is no longer confined to a thin boundary layer (Figs. 8d and 9d) and thus the mean square law fails. We conclude that the vorticity picture, ignored in most published reports, is essential in the understanding of cavity flow.

ACKNOWLEDGMENTS

The work of William D. McQuain, Calvin J. Ribbens, and Layne T. Watson was supported in part by Department of Energy grant DE-FG05-88ER25068 and Air Force Office of Scientific Research grant 89-0497. The computations were done on a Cray 2 and Cray Y-MP C90 at the National Energy Research Supercomputer Center, whose support we gratefully acknowledge.

REFERENCES

1. G. K. Batchelor, On steady laminar flow with closed streamlines at large Reynolds number, *J. Fluid Mech.*, **1**, 177 (1956).
2. O. R. Burggraf, Analytical and numerical studies of the structure of steady separate flows, *J. Fluid Mech.*, **24**, 113 (1966).

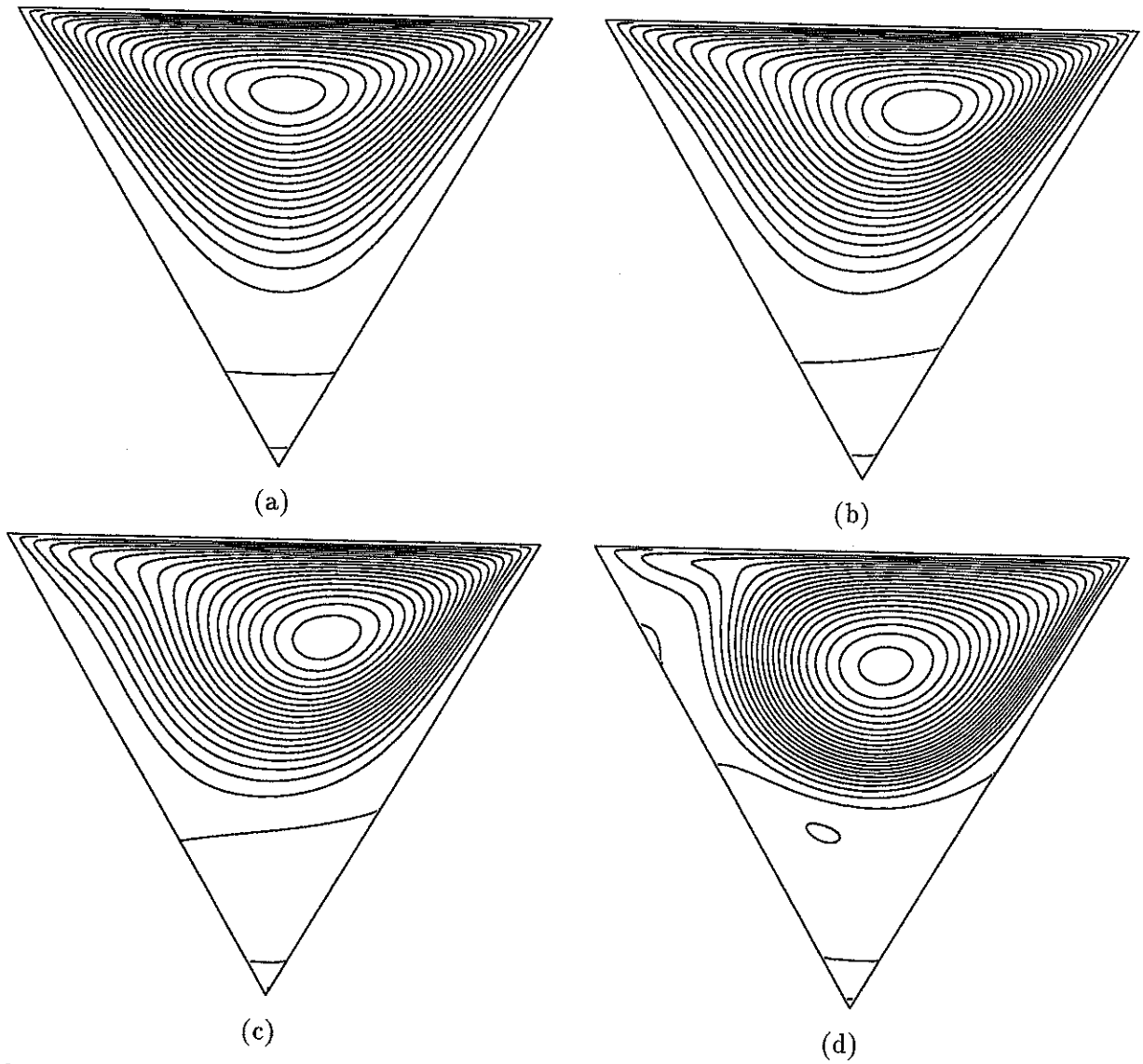

FIG. 5. Streamline patterns for the triangle, $\delta=\sqrt{3}$, for R=1 (a), R=50 (b), R=100 (c), and R=500 (d).

3. U. Ghia, K. N. Ghia and C. T. Shin, High-Re solutions for incompressible flow using the Navier-Stokes equations and a multi-grid method, *J. Comp. Phys.*, **48**, 387 (1982).
4. R. Schreiber and H. B. Keller, Driven cavity flows by efficient numerical techniques, *J. Comp. Phys.*, **49**, 310 (1983).
5. S. Y. Tuann and M. D. Olson, Review of computing methods for recirculating flow, *J. Comp. Phys.*, **29**, 1 (1978).
6. K. Gustafson and K. Halasi, Vortex dynamics of cavity flows, *J. Comp. Phys.*, **64**, 279 (1986).
7. C. N. Savvides and J. H. Gerrard, Numerical analysis of the flow through a corrugated tube with application to arterial prothesis, *J. Fluid Mech.*, **138**, 129–160 (1984).
8. E. M. Sparrow and M. Charmchi, Heat transfer and fluid flow characteristics of spanwise periodic corrugated ducts, *Int. J. Heat Mass Trans.*, **23**, 471–481 (1980).
9. C. J. Ribbens, C.-Y. Wang, L. T. Watson, and K. A. Alexander, Vorticity induced by a moving elliptic belt, *Computer Fluids*, **20**, 111 (1991).
10. R. Schreiber and H. B. Keller, Spurious solutions in driven cavity calculations, *J. Comp. Phys.*, **49**, 165 (1983).
11. C. J. Ribbens, L. T. Watson, and C.-Y. Wang, Steady viscous flow in a triangular cavity, Tech. Rep. 92–21, Dept. of Computer Sci., Virginia Polytechnic Inst. and State Univ., Blacksburg, VA, 1992.
12. S. Wolfram, *Mathematica*, Redwood City, California (1988).
13. F. Pan and A. Acrivos, Steady flows in rectangular cavities, *J. Fluid Mech.*, **28**, 643 (1967).
14. R. D. Mills, On the closed motion of a fluid in a square cavity, *J. Roy Aero. Soc.*, **69**, 116 (1965).
15. S. Timoshenko and J. N. Goodier, *Theory of Elasticity, 2nd Ed.*, McGraw-Hill, (1951).

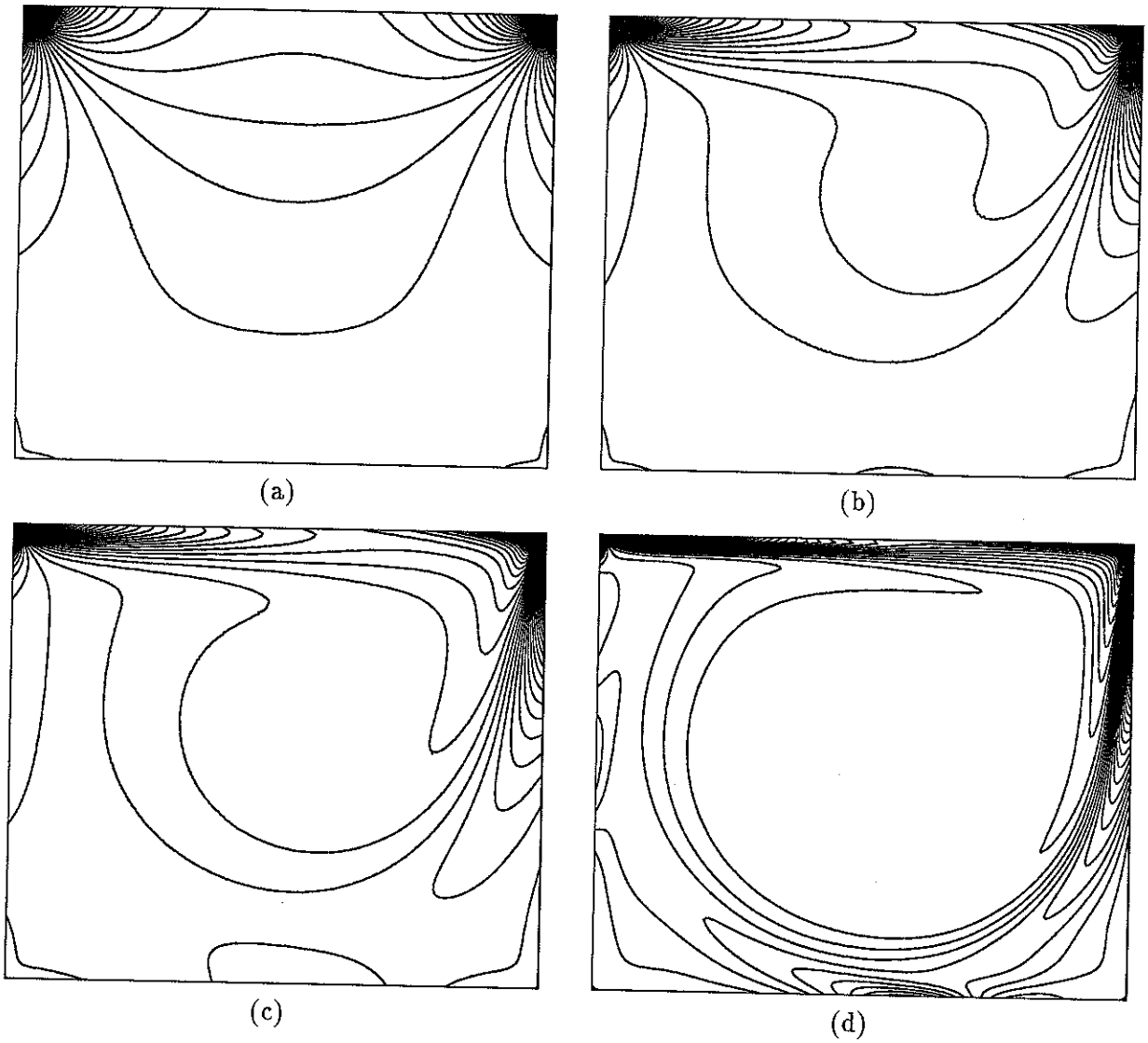

FIG. 6. Vorticity distribution for the rectangle, δ=0, for R=1 (a), R=50 (b), R=100 (c), and R=500 (d).

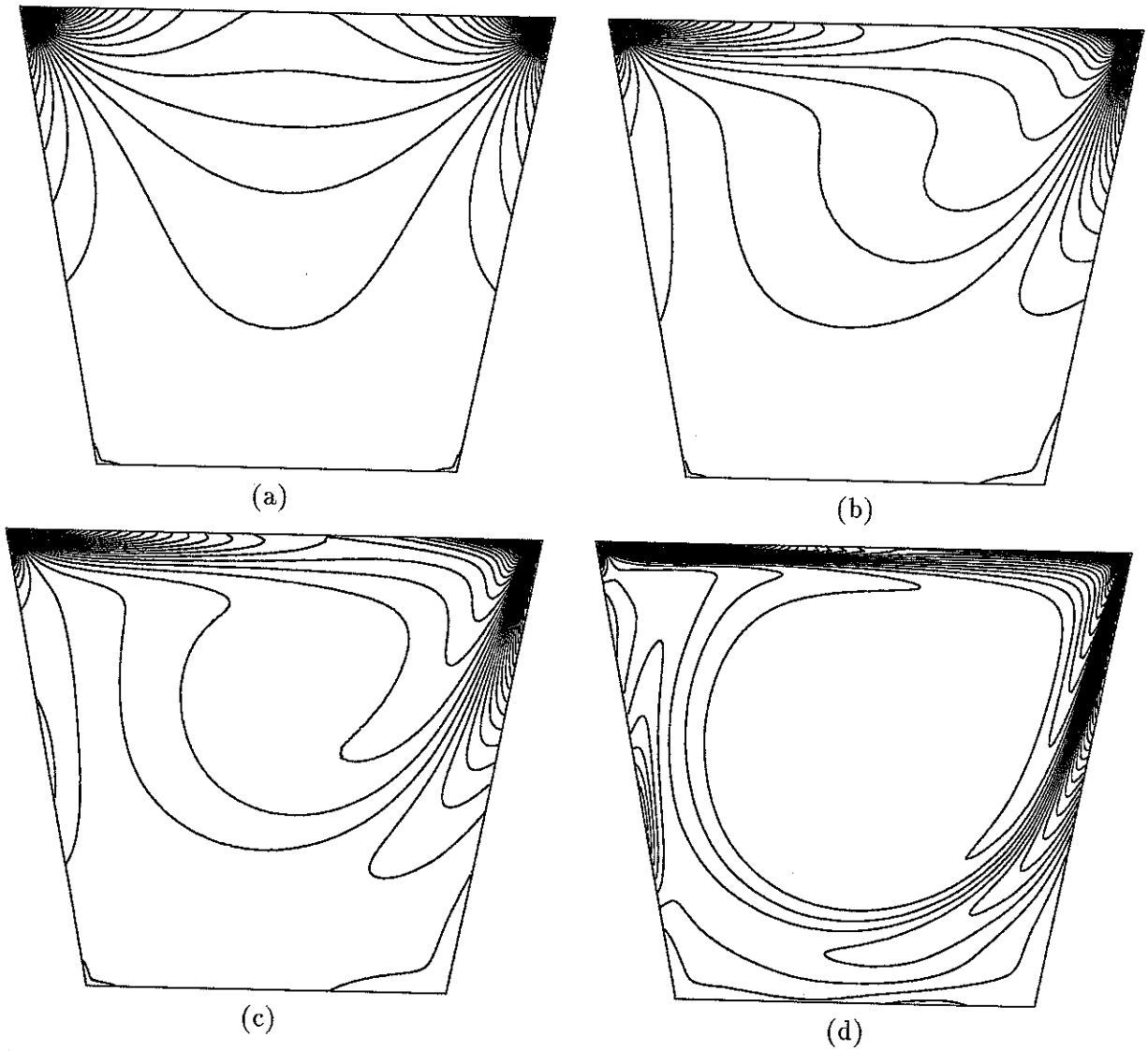

FIG. 7. Vorticity distribution for the trapezoid, $\delta=1/\sqrt{3}$, for R=1 (a), R=50 (b), R=100 (c), and R=500 (d).

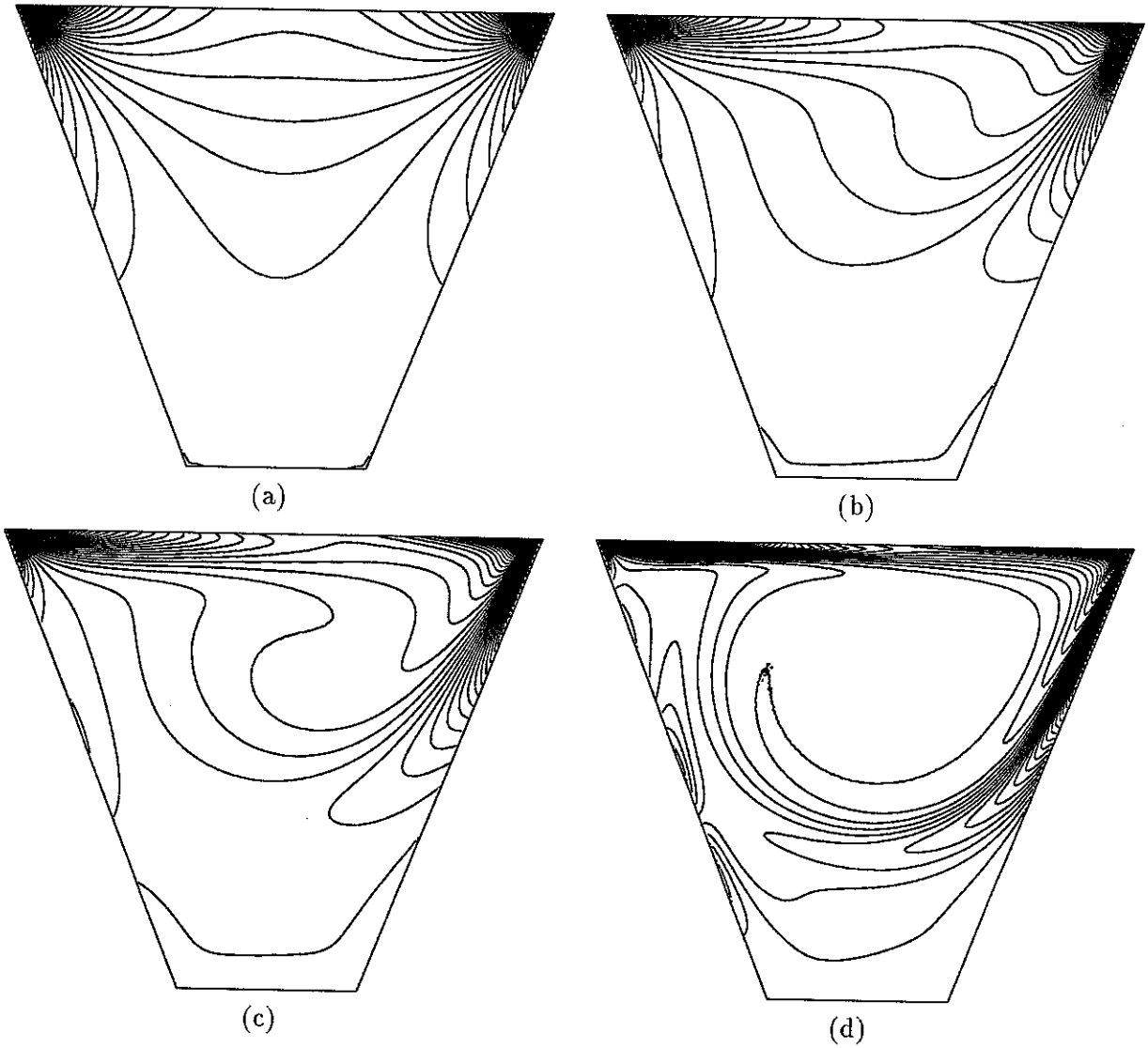

FIG. 8. Vorticity distribution for the trapezoid, $\delta=2/\sqrt{3}$, for R=1 (a), R=50 (b), R=100 (c), and R=500 (d).

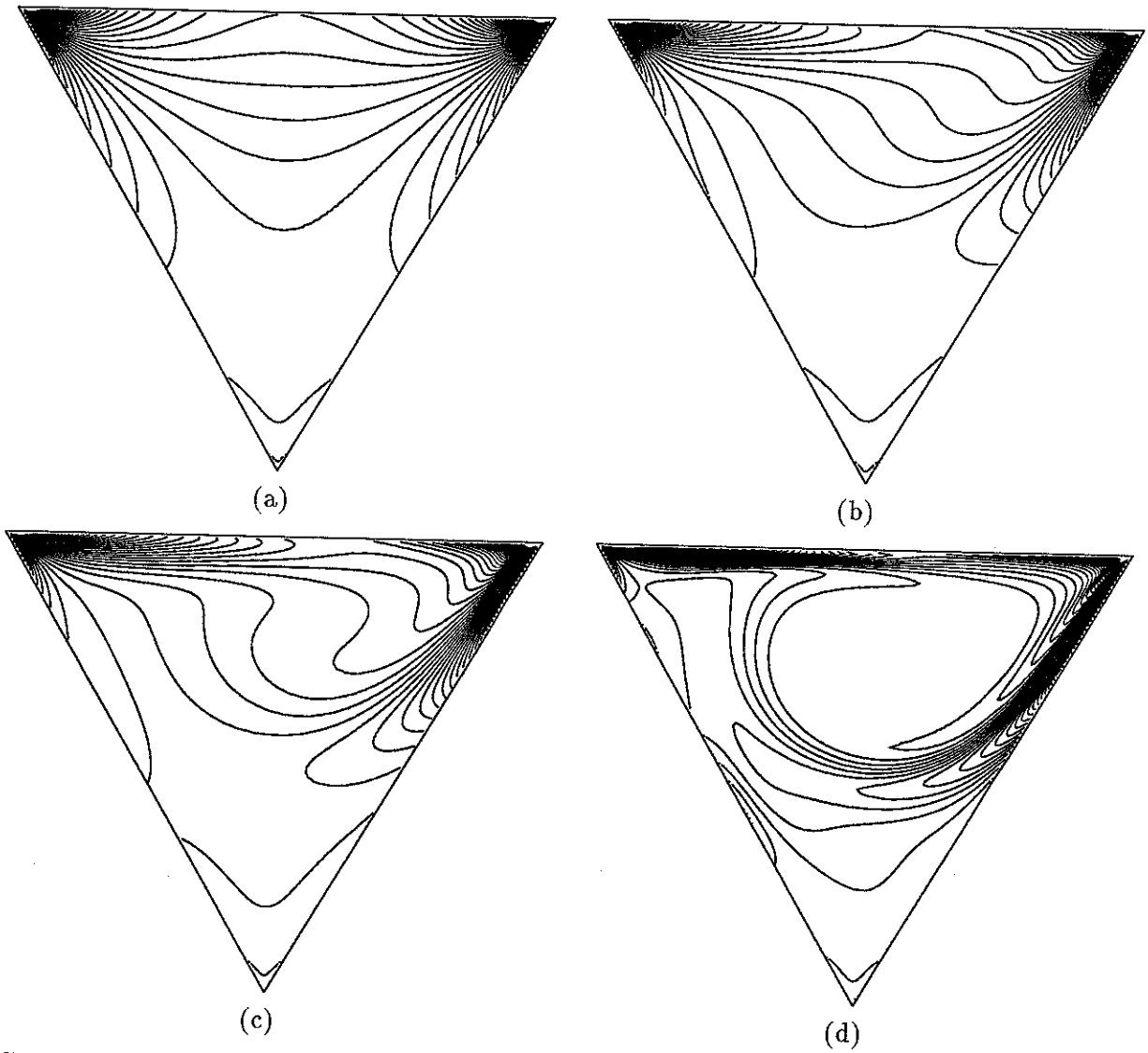

FIG. 9. Vorticity distribution for the triangle, $\delta=\sqrt{3}$, for R=1 (a), R=50 (b), R=100 (c), and R=500 (d).

APPENDIX I

The (i,j) entry in the templates below is the coefficient α_{ij} of $\Psi(x+ih, y+jh)$ in the finite difference approximation $\sum_{i,j=-2}^{2} \Psi(x+ih, y+jh)$ to a particular partial derivative of Ψ at (x,y).

$$\Psi_x : \frac{1}{2h}\begin{bmatrix} & 0 & 0 & & \\ 0 & 0 & 0 & 0 & \\ 0 & -1 & 0 & 1 & 0 \\ & 0 & 0 & 0 & 0 \\ & & 0 & 0 & \end{bmatrix}, \qquad \Psi_y : \frac{1}{2h}\begin{bmatrix} & 0 & 0 & & \\ 0 & 0 & 1 & 0 & \\ 0 & 0 & 0 & 0 & 0 \\ & 0 & -1 & 0 & 0 \\ & & 0 & 0 & \end{bmatrix},$$

$$\Psi_{xx} : \frac{1}{h^2}\begin{bmatrix} & 0 & 0 & & \\ 0 & 0 & 0 & 0 & \\ 0 & 1 & -2 & 1 & 0 \\ & 0 & 0 & 0 & 0 \\ & & 0 & 0 & \end{bmatrix}, \qquad \Psi_{xy} : \frac{1}{4h^2}\begin{bmatrix} & 0 & 0 & & \\ 0 & -1 & 0 & 1 & \\ 0 & 0 & 0 & 0 & 0 \\ & 1 & 0 & -1 & 0 \\ & & 0 & 0 & \end{bmatrix},$$

$$\Psi_{yy} : \frac{1}{h^2}\begin{bmatrix} & 0 & 0 & & \\ 0 & 0 & 1 & 0 & \\ 0 & 0 & -2 & 0 & 0 \\ & 0 & 1 & 0 & 0 \\ & & 0 & 0 & \end{bmatrix}, \qquad \Psi_{xxx} : \frac{1}{2h^3}\begin{bmatrix} & 0 & 0 & & \\ 0 & 0 & 0 & 0 & \\ -1 & 2 & 0 & -2 & 1 \\ & 0 & 0 & 0 & 0 \\ & & 0 & 0 & \end{bmatrix},$$

$$\Psi_{xxy} : \frac{1}{2h^3}\begin{bmatrix} & 0 & 0 & & \\ 0 & 1 & -2 & 1 & \\ 0 & 0 & 0 & 0 & 0 \\ & -1 & 2 & -1 & 0 \\ & & 0 & 0 & \end{bmatrix}, \qquad \Psi_{xyy} : \frac{1}{2h^3}\begin{bmatrix} & 0 & 0 & & \\ 0 & -1 & 0 & 1 & \\ 0 & 2 & 0 & -2 & 0 \\ & -1 & 0 & 1 & 0 \\ & & 0 & 0 & \end{bmatrix},$$

$$\Psi_{yyy} : \frac{1}{2h^3}\begin{bmatrix} & 0 & 1 & & \\ 0 & 0 & -2 & 0 & \\ 0 & 0 & 0 & 0 & 0 \\ & 0 & 2 & 0 & 0 \\ & & -1 & 0 & \end{bmatrix}, \qquad \Psi_{xxxx} : \frac{1}{h^4}\begin{bmatrix} & 0 & 0 & & \\ 0 & 0 & 0 & 0 & \\ 1 & -4 & 6 & -4 & 1 \\ & 0 & 0 & 0 & 0 \\ & & 0 & 0 & \end{bmatrix},$$

$$\Psi_{xxxy} : \frac{1}{2h^4}\begin{bmatrix} & 0 & 0 & & \\ -1 & 3 & -3 & 1 & \\ 1 & -4 & 6 & -4 & 1 \\ & 1 & -3 & 3 & -1 \\ & & 0 & 0 & \end{bmatrix}, \qquad \Psi_{xxyy} : \frac{1}{h^4}\begin{bmatrix} & 0 & 0 & & \\ 0 & 1 & -2 & 1 & \\ 0 & -2 & 4 & -2 & 0 \\ & 1 & -2 & 1 & 0 \\ & & 0 & 0 & \end{bmatrix},$$

$$\Psi_{xyyy} : \frac{1}{2h^4}\begin{bmatrix} & -1 & 1 & & \\ 0 & 3 & -4 & 1 & \\ 0 & -3 & 6 & -3 & 0 \\ & 1 & -4 & 3 & 0 \\ & & 1 & -1 & \end{bmatrix}, \qquad \Psi_{yyyy} : \frac{1}{h^4}\begin{bmatrix} & 0 & 1 & & \\ 0 & 0 & -4 & 0 & \\ 0 & 0 & 6 & 0 & 0 \\ & 0 & -4 & 0 & 0 \\ & & 1 & 0 & \end{bmatrix}.$$

APPENDIX II

At high Reynolds numbers the vorticity of the core of the eddy is approximately constant. Batchelor [1] proposed a mean square law to relate core vorticity with boundary velocities. The flow in the core is governed by

$$\nabla^2 \psi = C, \tag{A1}$$

where C is the constant vorticity value. The method is to solve equation (A1) analytically for a specific geometry. The constant C is obtained from the relation

$$\oint \left[(\psi_\xi)^2 + (\psi_\eta)^2\right]\, ds = \oint U^2(s)\, ds, \tag{A2}$$

where s is the arc length along the boundary and U is the boundary velocity.

A. The rectangle of size $2\sqrt{3} \times 3$.

The Poisson equation for a rectangle has been solved before (e.g., in Timoshenko and Goodier [15]), using a simpler formulation. Let Cartesian axes (ξ, η) be located at the center of the rectangle. The boundary conditions are $\psi = 0$ on $\xi = \pm\sqrt{3}, \eta = \pm 3/2$. Set $\psi = C\phi$, where

$$\phi(\xi,\eta) = \frac{\eta^2}{2} - \frac{9}{8} + \sum_{n=1}^{\infty} A_n \cos\left[(n-\tfrac{1}{2})\pi\frac{2\eta}{3}\right] \cosh\left[(n-\tfrac{1}{2})\pi\frac{2\xi}{3}\right] \tag{A3}$$

which satisfies equation (A1) and the boundary conditions on $\eta = \pm 3/2$. The other boundary conditions yield

$$\frac{9}{8} - \frac{\eta^2}{2} = \sum_{n=1}^{\infty} A_n \cosh\left[(n-\tfrac{1}{2})\frac{2\pi}{\sqrt{3}}\right] \cos\left[(n-\tfrac{1}{2})\pi\frac{2\eta}{3}\right] \tag{A4}$$

The constants A_n are obtained by Fourier inversion

$$A_n = \frac{9(-1)^{n+1}}{2(n-\frac{1}{2})^3\pi^3} \operatorname{sech}\left[\frac{2\pi}{\sqrt{3}}(n-\tfrac{1}{2})\right]. \tag{A5}$$

From equation (A2) we find

$$C^2 = \frac{\sqrt{3}}{2}\left\{\int_0^{3/2}\left[\phi_\xi(\sqrt{3},\eta)\right]^2 d\eta + \int_0^{\sqrt{3}}\left[\phi_\eta(\xi,3/2)\right]^2 d\xi\right\}^{-1}. \tag{A6}$$

The value of C is computed by truncating the infinite series in equation (A3) to a finite number of terms and using a symbolic algorithm (e.g., Mathematica) for equation (A6). Four-digit accuracy is obtained for 10 terms. We find $C = 0.6071$.

B. The equilateral triangle with sides $2\sqrt{3}$.

An exact solution exists for the equilateral triangle:

$$\psi = \frac{C}{12}(\eta - 1)(\eta + 2 - \sqrt{3}\xi)(\eta + 2 + \sqrt{3}\xi). \tag{A7}$$

Using symmetry, equation (A2) reduces to

$$3\int_{-\sqrt{3}}^{\sqrt{3}}\left[\psi_\eta(\xi,1)\right]^2\, d\xi = 2\sqrt{3}. \tag{A8}$$

This gives $C = \sqrt{10}/3 = 1.054$.